Eur. Phys. J. B **27**, 103–109 (2002)
DOI: 10.1140/epjb/e20020134

THE EUROPEAN PHYSICAL JOURNAL B
EDP Sciences

Dipolar coupling effect in magnetic bilayer system

M. Labrune[1,a] and H. Niedoba[2]

[1] Laboratoire PMTM; CNRS - Université Paris-13, 93430 Villetaneuse, France
[2] Laboratoire de Magnétisme et d'Optique, CNRS-Université de Versailles, St. Quentin en Yvelines, 78035 Versailles, France

Received 12 December 2001

Abstract. Equilibrium micromagnetic structures in a bilayer system composed of two thin cobalt films separated by a non magnetic spacer are systematically analysed. These 2D magnetization distributions are obtained by numerical computations according to different set of magnetic and geometric parameters. The coupling effect due to the dipolar long range interaction (or stray-field effect) between the two Co layers is studied through the evolution of the magnetic pattern in the stack with or without an applied field and compared to a continuous film of same thickness. Special attention is paid to the hysteresis process in a bilayer. Even though the general aspect of the magnetization distribution looks like a Landau-Lifshitz structure, the absence of any core in the vortex of the magnetic structure is analysed in relation to a possible disappearence of (topological) hysteresis.

PACS. 75.60.Ch Domain walls and domain structure – 75.70.Cn Interfacial magnetic properties (multilayers, superlattices) – 75.50.Ss Magnetic recording materials

1 Introduction

Recently special attention has been paid to Co multilayers [1]. The possible occurrence of a large perpendicular anisotropy makes Co stacks attractive candidates for high data storage media. On the other hand, this peculiar attention is also partly due to many interesting and practical applications as GMR sensors [2,3] related to the nature of the interlayer exchange coupling effects. Our past studies [4] devoted to a more simple system: Co/Cr/Co were mainly concerned with the ferro- and antiferromagnetic coupling in this stack composed of two polycrystalline Co layers 20 nm thick. As no buffer layer was used to grow cobalt, the observed perpendicular anisotropy was always too weak to deviate magnetization from its in-plane orientation and the effects associated with the in-plane anisotropy induced during deposition were studied. The corresponding micromagnetic analysis of wall structures between in-plane domains can be found in [5].

The aim of this paper is to study theoretically the influence of the perpendicular anisotropy on the elementary system composed of two Co magnetic layers 20 nm thick (Fig. 1). Predictive results are given with the help of micromagnetic simulation assuming a perpendicular anisotropy strong enough to support, at least, weak stripe pattern [6] (see also Fig. 2b for example) and with no interlayer exchange coupling. All these results will be used in a forthcoming article [7] devoted to the analysis of the transverse biased susceptibility in such films. The present calculation provides the equilibrium magnetization distributions first step for the knowledge of the dynamical susceptibility which corresponds to the response of the static configuration to a weak uniform excitation.

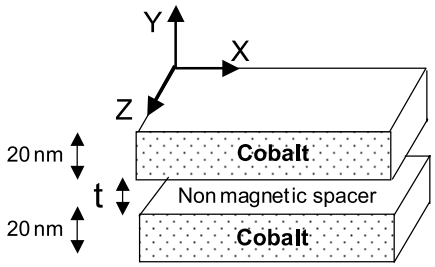

Fig. 1. Bilayer geometry.

This paper is organized as follows: The bases of the numerical method are outlined in Section 2. The magnetic parameters and the geometry used are given in Section 3. A general overview of the main differences between the static remanent magnetization profile of a bilayer with the expected profiles for a continuous film 20 nm and 40 nm thick respectively are given in Section 4. Details of the evolution of the magnetic pattern in a bilayer as a function of the non magnetic spacer thickness is proposed in Section 5 while the effect of a longitudinal applied field for different anisotropy values is discussed in Section 6. Special attention is paid to the hysteresis process in bilayers (Sect. 7). In particular the absence of any core in the

[a] e-mail: ml@lpmtm.univ-paris13.fr

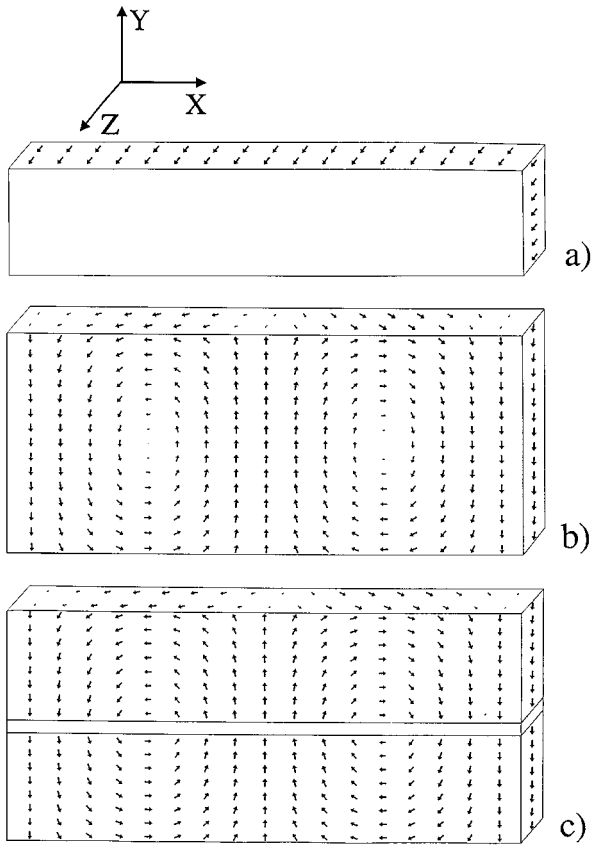

Fig. 2. 3d magnetization profiles of a) a single continuous layer of cobalt 20 nm thick, b) a single layer 42 nm thick and c) a bilayer (Co 20 nm/spacer 2.1 nm/Co 20 nm). The scale along the OX axis is normalized to one period 2W in case b and c (the size of the slabs are assumed infinite along OZ).

vortex of the magnetic structure due to the broken exchange in the mid-stack is studied in view of the possible disappearance of (topological) hysteresis [6].

2 Numerical method

The code used in the present calculations minimizes the torque associated with the effective field acting on the magnetization: $\boldsymbol{\Gamma} = \mathbf{M} \times \mathbf{H}_{\text{eff}}$. $\mathbf{H}_{\text{eff}}$ is the effective field with contributions from the exchange, bulk anisotropy, applied and demagnetizing field energies. At each iteration step the magnetization is slowly rotated towards the effective field direction. This method, neglecting the precession, describes only equilibrium states which are said to be reached when the reduced torque $\|\boldsymbol{\Gamma}/2\pi M_S\|$ is everywhere smaller than 10^{-4} times the anisotropy field $H_K = 2K/M_S$.

The expected periodic stripe domains are assumed to be elongated along the OZ axis. Therefore, the three components of the magnetization vector $\mathbf{m}(\mathbf{r}) = \mathbf{M}(\mathbf{r})/M_S$ do not depend on the Z coordinate. In cross section OX, OY (the Y axis being normal to the plane of the stack, see geometry in Fig. 1) and for each magnetic layer, the continuous magnetization distribution $\mathbf{m}$ is reduced to a finite number of vectors located at the nodes of a regular (Cartesian) grid of periods a and b, limited to one period $2W$ of the magnetic pattern. The a and b parameters are chosen such that the ratios ℓ/a and ℓ/b should remain larger than 5, where ℓ is the smallest characteristic length of the problem: either the Bloch wall width $\pi\sqrt{\frac{A}{K}}$ or the exchange length $\pi\sqrt{\frac{A}{2\pi M_S^2}}$.

Along surfaces of each magnetic layer in the stack and in the absence of surface anisotropy as well as any interlayer exchange coupling, the magnetization should be stationary. Therefore, the surface condition reads:

$$\frac{\partial \mathbf{m}}{\partial n} = \mathbf{0} \cdot \tag{1}$$

The present calculations use a scheme assuming a constant magnetization within each prism ($a \times b$) leading to charged surfaces [8]. The calculation provides an expression for the average value of the demagnetizing field within each prism. Finally, the code used had been previously adapted [6] in order to take into account the periodic nature of the magnetization distribution: $\mathbf{m}(x, y) = \mathbf{m}(x + P.2W, y)$, where P is an integer. Therefore, the period $2W$ is an additional variable in the minimization process. Several calculations differing in the sole $2W$ value have to be undertaken so as to get the lowest energy configuration providing the equilibrium domain period. Finally, in order to save computational time, the following symmetry with respect to the mid-plane of the full stack ($y = 0$) is used: $m_X(x, y) = -m_X(x, -y)$; $m_Y(x, y) = +m_Y(x, -y)$ and $m_Z(x, y) = +m_Z(x, -y)$.

3 Magnetic parameters and geometry

The present numerical simulations are restricted to the bilayer system composed of two Cobalt layers 20 nm thick each separated by a non-magnetic spacer of varying thickness from 0.7 to 9 nm. The magnetic parameters used correspond to that usually mentioned for hcp cobalt thin epitaxial films [9] namely: magnetization $M = 1400$ emu/cm^3, uniaxial anisotropy constant $K_1 = 5 \times 10^6$ erg/cm^3, the C (hexagonal) axis being perpendicular to the film plane (OY axis according to our convention, see Fig. 1). The anisotropy contribution to the free energy has the simple form:

$$E_{\text{ani}} = K_1 \left(1 - m_y^2\right) \cdot$$

The exchange constant A in cobalt is not well defined. Various values ranging from A $= 3.2 \times 10^{-6}$ erg/cm [10] to A $= 1 \times 10^{-6}$ erg/cm [9] can be found in the literature. Here we used an intermediate value A $= 1.8 \times 10^{-6}$ erg/cm. The characteristic lengths mentioned in Section 2 can then be calculated. One found $\ell_W = \pi\sqrt{\frac{A}{K}} = 19$ nm and $\ell_{ex} = \pi\sqrt{\frac{A}{2\pi M_S^2}} = 12$ nm while the quality factor ratio Q defined as the anisotropy field

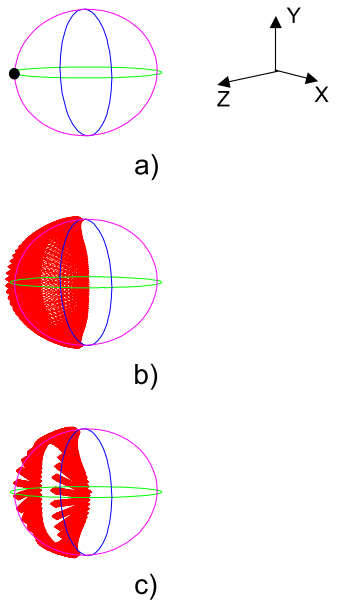

Fig. 3. Magnetization mapping onto the unit sphere: a) monolayer of cobalt 20 nm thick, b) monolayer 42 nm thick and c) case of a bilayer (Co 20 nm/ spaceur $t = 3.5$ nm / Co 20 nm).

$H_K = 2K_1/M_S = 7.1$ kOe over the demagnetizing field $H_d = 4\pi M_S = 17.6$ kOe amounts to $Q = \frac{K_1}{2\pi M_S^2} = 0.4$. It is well known that a minimum film thickness, D_{cr}, is needed to get stripe domains in presence of a perpendicular anisotropy. Below this critical film thickness, only strictly in-plane orientation of magnetization is stable. A good criterion [11] for the appearance of stripe domains in a single film of thickness D is given by the ratio $R = \frac{D}{2\pi\sqrt{A/K}}$. For moderate Q values ($Q < 0.1$), stripe pattern occurs for $R > 1$ (*i.e.* $D > D_{cr} = 2\pi\sqrt{A/K}$). However, R decreases towards zero when the value of the quality factor reaches unity. In the case of a single cobalt layer 20 nm thick and according to its magnetic parameters given above, the ratio R is much lower than unity ($R = 0.53$), therefore no stripes at all are expected. The magnetization should remain in the plane of the sample. On the contrary, for $D = 42$ nm, $R = 1.12$ and a stripe pattern is expected. Therefore, one of the questions to be answered is what does happen when we put together two Co layers 20 nm thick each, leaving between them only a small nonmagnetic gap.

4 Bilayer versus monolayer: a general overview

Figure 2 exhibits the magnetization profiles for three different cases: single films 20 nm and 42 nm thick and a bilayer. Everywhere, in this figure, the length of the arrows is proportional to the component of the magnetization vector in the corresponding plane. For a continuous film 20 nm thick (Fig. 2a) the magnetization stays in the (XOZ) plane parallel to the film surface, more precisely along the OZ axis. Therefore, in a cross section of the film (plane XOY) the magnetization points towards us (perspectice effect) what explains the lack of any arrow in this part of the drawing. This numerical result is in agreement with the previous remark done in Section 3. According to the magnetic parameters used, the critical thickness Dcr above which stripe pattern may occur is, according to diagram in reference [11], $D_{cr} = 26$ nm. Figure 2b corresponds to the expected pattern for a continuous film 42 nm thick in which stripe domains elongated along the OZ axis occur. The equilibrium domain width along OX (half period of the structure) is equal to $W = 52.5$ nm while the longitudinal remanent magnetization amounts to $\langle m_z \rangle = 0.36$. This pattern resembles a Landau-Lisfchitz structure with basic domains magnetized along the main easy axis (OY). Closure areas in the vicinity of the top and bottom surfaces ensure a virtually stray field free magnetization distribution with alternate flux circulations. However, the essential feature of the magnetic pattern is its unwinding character. In other words, the magnetization pattern can be viewed as piled-up vortices, where, in the core of all of them the magnetization points towards $+OZ(m_Z = +1)$. Therefore, under the action of a field applied along $+OZ$, the transition towards the saturated state can be obtained continuously (*i.e.* second-order phase transition). Starting from the opposite saturated state, another structure can be obtained where, the core of all the vortexes points towards $-OZ$ ($m_Z = -1$). Finally, Figure 2c shows the stripe pattern obtained for a bilayer composed of two films of cobalt 20 nm thick each separated by a non-magnetic spacer 2.1 nm thick: (Co 20 nm/spacer 2.1 nm/Co 20 nm). The equilibrium stripe width is equal to $W = 63$ nm and the longitudinal remanent magnetization $\langle m_z \rangle = 0.1$ – a value significantly much smaller than that observed in the single layer case with equivalent total thickness of magnetic material. In the bilayer, in spite of the discontinuous aspect of the magnetic sample, the overall configuration shows a pronounced magnetization circulation. However, one can notice that the core of the vortex, which corresponds to $m_x = m_y = 0$ and $m_z = 1$, is no more present. On the contrary, an abrupt variation of the transverse in-plane component m_x is observed instead of the vortex core when crossing the spacer what is favoured by the absence of any interlayer exchange force. Furthermore, in between "up" and "down" domains, the flux closure is ensured *via* wall structure characterized by its Néel aspect. Both effects explain as well the reduced value of $\langle m_z \rangle$ in the case of a bilayer compared to the single film's one. A different way of presenting these three magnetization distributions is shown in Figure 3, using the unit sphere also referred to as the Feldkeller's sphere [12]. For the cobalt single layer 20 nm thick, only one direction of magnetization is used: **m** (0,0,1), and the corresponding point in the unit sphere is indicated in Figure 3a. In the case of the weak stripe pattern corresponding to the cobalt film 42 nm thick, the magnetization distribution is leading only to a partial coverage of the unit sphere (Fig. 3b). More precisely, only a part of the hemisphere including the (0,0,1) pole is covered

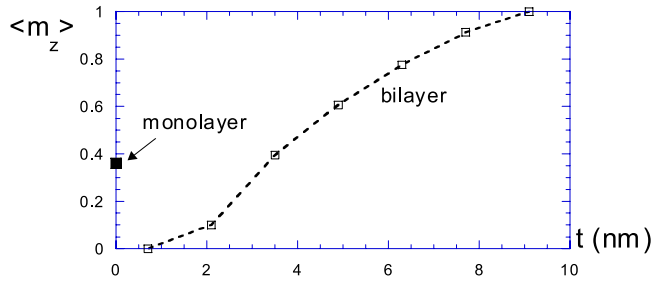

Fig. 4. Variation of the average longitudinal component of magnetization $\langle m_Z \rangle$ *versus* the thickness t of the non magnetic spacer. The corresponding value for a single film 42 nm thick is given in $t = 0$.

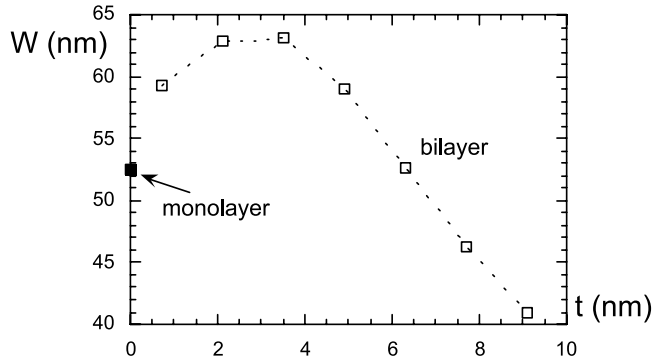

Fig. 5. Variation of the domain width W (half period of the magnetic structure) *versus* the thickness t of the non magnetic spacer. The corresponding value for a single film 42 nm thick is given in $t = 0$. In the figure the ordinate W range from 40 to 65 nm.

(see also Ref. [6]). However, the structure obtained for the bilayer (Fig. 3c) differs from the previous one. The directions of **m** close to OZ axis are missing in this structure. A general overview of the magnetization profiles in multilayer systems exhibiting a perpendicular anisotropy can be found in [10,13]. Compared to a single layer, the dominating features associated to a multilayer come to light as soon as one analyses the magnetic properties of a bilayer. But when increasing the number of layers, it can be shown (see Ref. [14]) that above a threshold value for the number of magnetic layers in the stack, the onset of a vortex is observed accompanied by the emergence of a Bloch-like section through the central part of the film.

5 Evolution of the equilibrium magnetic pattern with increasing thickness of the spacer

Several calculations, using the same set of magnetic parameters have been done for different thickness of the spacer. The main results obtained in zero field are gathered in Figures 4 and 5. With increasing thickness of the spacer, the longitudinal component of magnetization m_Z averaged over one period of the pattern increases rapidly towards 1 (Fig. 4). For thin spacers, the pattern is characterized by a small value of $\langle m_z \rangle$. The magnetization

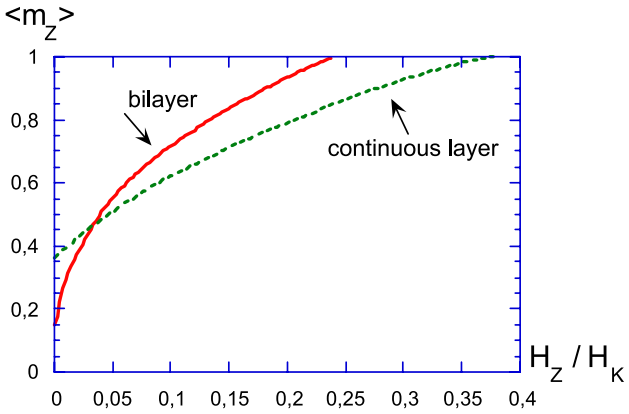

Fig. 6. Comparison of the behavior of the longitudinal magnetization component $\langle m_Z \rangle$ under an applied field H_Z for two different cases: a bilayer (Co 20 nm/ spacer $t = 2.1$ nm / Co 20 nm) and a continuous magnetic layer 42.1 nm thick.

prefers to stay in the transverse XOY plane: such an effect related to a Néel nature of the wall in each layer has been described in detail in references [10] and [14]. Furthermore, whatever the nonmagnetic spacer thickness is, the core of the vortex ($m_Z = 1$) observed in a continuous film doesn't exist anymore. One can notice that for thin spacers the average value $\langle m_z \rangle$ can be next to zero. These results must be understood under the assumption made in these calculations of absence of any exchange coupling between the layers. With such condition, the behavior of the stack in case of vanishing thickness of the nonmagnetic spacer differs from that of a (magnetic) continuous single film. Now, for thicker spacers, the bilayer is magnetized uniformly along OZ. This last pattern is reached for a thickness of the spacer $t \approx 9.2$ nm. Above this value, the stray field effect is not strong enough to generate stripe pattern and each layer in the stack acts individually as a single layer depicted in Figure 2a. Finally, the variation of the domain width is reported in Figure 5. For small nonmagnetic layer thickness values, an important increase of stripe width occurs compared to that of an equivalent monolayer. Similar behaviour has been reported for multilayers (Ref. [10] and [14]). Farther increase of **t** induces a large decrease of W. The collapse of the stripe pattern described above is reached just before the transition occurs while a finite value of W, close to the total magnetic thickness in the bilayer, is observed just before.

6 Effect of a longitudinal applied field

To compare the effect of a magnetic field on a bilayer and a single layer, stripe domains were investigated when applying field (H_Z) along the stripe direction. The results obtained for: a) a bilayer (Co 20 nm/spacer 2.1 nm/Co 20 nm) and b) a continuous magnetic film of equal total thickness 42.1 nm are shown in Figure 6. Although the remanent magnetization in zero field is lower in the bilayer case, the saturation is reached more easily than for a single layer. The applied field aligns the magnetization along the

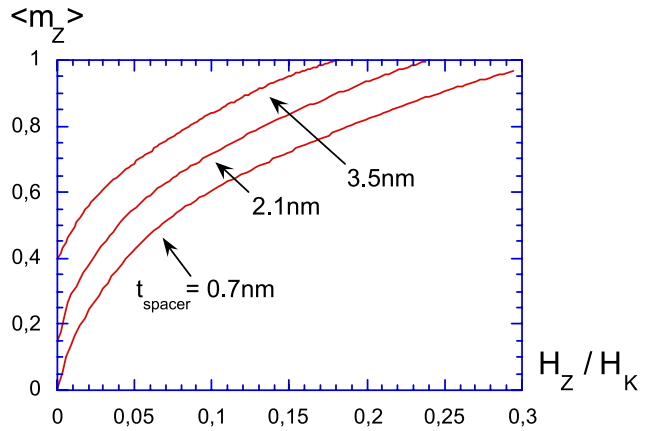

Fig. 7. Variation of the average longitudinal magnetization $\langle m_Z \rangle$ of a bilayer (Co 20 nm/ spacer t / Co 20 nm) under an applied field H_Z for three different thicknesses t of the non magnetic spacer.

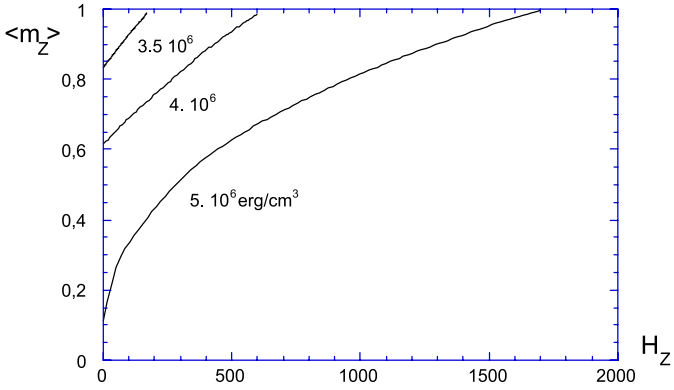

Fig. 8. Variation of the average longitudinal magnetization $\langle m_Z \rangle$ of a bilayer (Co 20 nm/ spacer 2.1 nm / Co 20 nm) under an applied field H_Z for three different values of the perpendicular anisotropy constant K_1.

OZ axis and consequently weakens the coupling between layers; this explains the ease of saturation for the bilayer. The effect of the spacer thickness on the magnetization curve is depicted in Figure 7. A thin spacer implies both a longitudinal remanent magnetization next to zero and a strong coupling between magnetic layers associated with a strong value of the saturation field. On the contrary, the thicker the spacer is, the higher is the value of the zero field remanent magnetization. In this case, the weakness of the coupling leads to a reduced value of the field needed to saturate the stack. Finally, the effect of the variation of the perpendicular uniaxial anisotropy constant on the magnetization process for a fixed geometry is depicted in Figure 8. Obviously, for a given geometry of the stack, a critical value of the anisotropy constant is needed below which no stripes occur. The corresponding values found for the quality factor Q and the characteristic thickness ratio $R = \frac{D}{2\pi\sqrt{A/K}}$, where D is assumed equal to the total magnetic thickness in the bilayer, are equal to ($Q = 0.4$; $R = 1.06$); (0.32; 0.95) and (0.28; 0.88) respectively. Inspection of the Q, R diagram in reference [11] shows that even in the last case which corresponds to the smallest value of the anisotropy constant used in the numerical calculation, stripe domains would be expected in a continuous layer too.

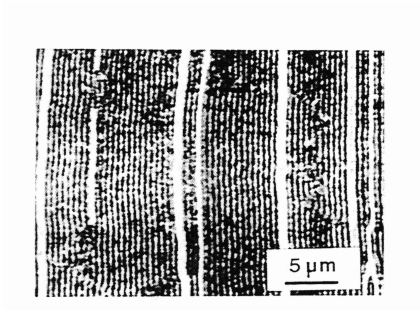

Fig. 9. Kerr micrograph showing the nucleation of new stripe domain at the magnetization reversal in a single layer of CoFeZr 3000 Å thick.

7 Topological aspect of the magnetization process

The nucleation of domain pattern starting from the saturated state, the knowledge of the hysteresis curve as well as the magnetization reversal are subjects of great interest in theory of ferromagnetism. However, theses processes, usually first order ones, are mostly governed by the presence of surface or volume defects in the sample. Therefore, theoretical treatments are in general far from being satisfactory. Such is not the case in the present situation when the applied field is directed along any in-plane direction. Even for a monolayer, the approach towards saturation is typical of a second order phase, continuous transition. As previously shown in Figure 3b, the magnetization distribution will only lead to a partial coverage of the unit sphere homotopic to a point corresponding to the saturated state. Then, the critical (saturation) field can be derived analytically from micromagnetic theory [15]. On the contrary, once the stripe pattern nucleated and, always in the case of a continuous monolayer, the magnetization reversal process remains a first order transition. In Figure 9 we show the Kerr micrograph which illustrates such a mechanism in a single amorphous CoZeFr layer. At the beginning of magnetization reversal, new stripe domains of opposite Kerr contrast (white on the Kerr micrograph) corresponding to opposite longitudinal magnetization direction are nucleated near the edges or defects in the sample and then expands over all the surface of the specimen. An analysis in terms of a space order parameter helps in the understanding of such a mechanism. Starting with the saturated state, and progressively decreasing the applied field leads to a gradual coverage of the Feldkeller's sphere (see Fig. 3b) which correspond to the stripe domain state.

When reversing the applied field, nearly all the directions of the 3D space may be found what correspond to

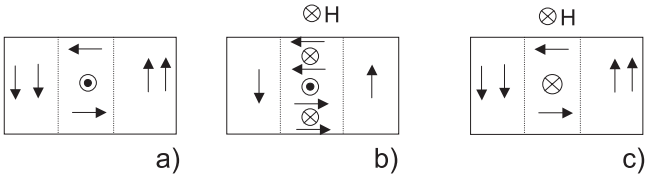

Fig. 10. Nucleation of a 2π line pair under the action of field applied along the $-OZ$ direction.

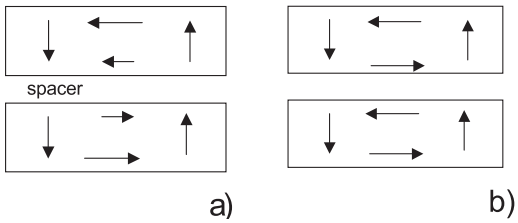

Fig. 12. Schematic magnetization distribution over half a period of the pattern in the case of: a) a strong demagnetizing coupling between layers and b) a weak coupling.

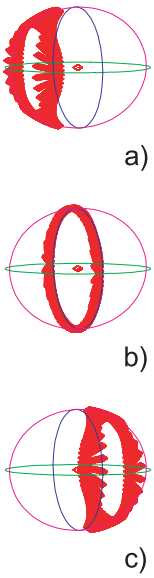

Fig. 11. Magnetization mapping onto the unit sphere in the case of (Co 20 nm/ spacer 0.7 nm / Co 20 nm) stack for three different value of the applied field: a) $H_z = +600$ Oe, b) $H_z = 0$ Oe and c) $H_z = -400$ Oe. The inset in Figure 3a reminds the corresponding geometry.

a full coverage of the unit sphere. There, no escape way is allowed to reduce this occupied area to a single point on the unit sphere and reach the opposite saturated state, except by introducing topological defects. Applying a field opposed to the wall magnetization may lead to the nucleation of a 2π Bloch line pair (cross Bloch lines) as shown in Figure 10 [16]. However, the injection of two Bloch points (two z-circulating, one convergent and the second one divergent according to the nomenclature described in [16]) is still necessary to cut the remaining circular Bloch line. In other words, there is no continuous transformation. The situation is different in a bilayer with thin spacer, as illustrated for a 20 nm/0.7 nm/20 nm stack in Figure 11. We see that the magnetization distribution covers only a small part of the unit sphere and that, from the very beginning of the nucleation process, the saturated direction ($m_z = +1$) is no more occupied. Therefore, a continuous way to reverse the magnetization does exist and no hysteresis occurs. However, such process is only applying for stacks with very thin spacer. As shown in Figure 4, the longitudinal remanent magnetization largely differs from zero for $t \geq 2$ nm, consequently, the magnetization reversal is hysteretic. In fact, the topological argument previously developed is still valid. Let us consider here the relative contribution of the exchange and demagnetizing terms and show that the demagnetizing term contributes especially for larger t. Figure 12a depicts the schematic magnetization distribution obtained in bilayers' cross section. In such situation, the magnetic flux is closed over the two layers. If we largely increase the thickness of the spacer, the theoretical opposite situation described in Figure 12b where the flux is closed inside each individual magnetic layer may occur. Such is also the case if we increase the thickness of each individual layer keeping t constant, see for example the magnetization distribution shown in Figure 13 corresponding to $R = 10$ and $Q = 0.04$ with $t = 3$ nm ($D = 250$ nm; $K = 2.5 \times 10^5$ erg/cm^3). In the present situation of a bilayer (20 nm Co / t /20 nm Co) with t small (Fig. 14a), the demagnetizing field is mainly up and down and strongly limited to the spacer area. With a thicker spacer, however, the demagnetizing field area may develop (Fig. 14b) where the magnetization direction near the interface in the top and bottom layers is opposite to the demagnetising field along $+0X$ or $-OX$ (for the top layer, see Fig. 14c). When reversing the applied field H_a, now applied along $-OZ$, and at the same position in the film, the magnetization in the top layer, due to exchange interaction with neighbouring spins should turn clockwise mainly in the XOZ plane and then overcome an energy barrier when being along $-OX$ (*i.e.* opposite to the local demagnetizing field) before reaching the situation depicted in Figure 14d. This mechanism may explain the hysteretic behaviour noticed on bilayers with large non-magnetic thickness spacer.

8 Conclusion

2D numerical simulations of stripe domains in a cobalt bilayer, built of cobalt layers 20 nm thick each, and separated by a non magnetic spacer of various thickness, have been done.

These results are compared to what is expected for a continuous single layer of cobalt either 20 nm or 40 nm thick exhibiting the same perpendicular anisotropy.

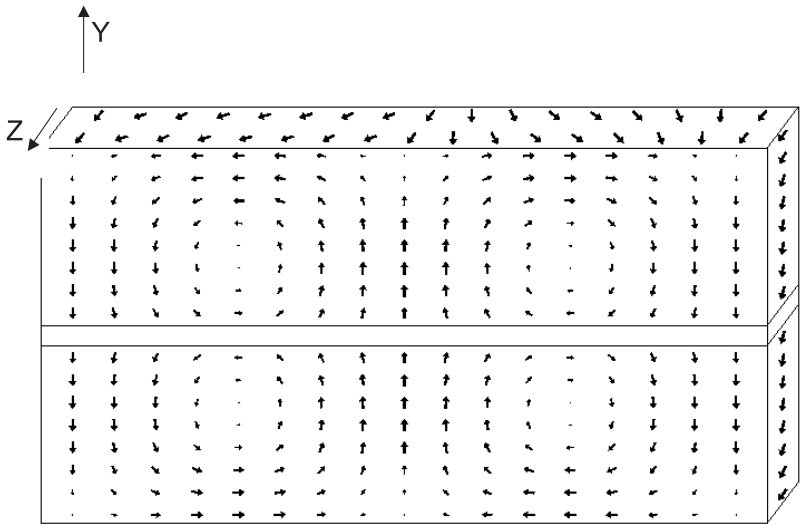

Fig. 13. 3d magnetization profile of a bilayer (Co 120 nm/spaceur 3 nm/Co 120 nm) with low quality factor $Q = 0.04$.

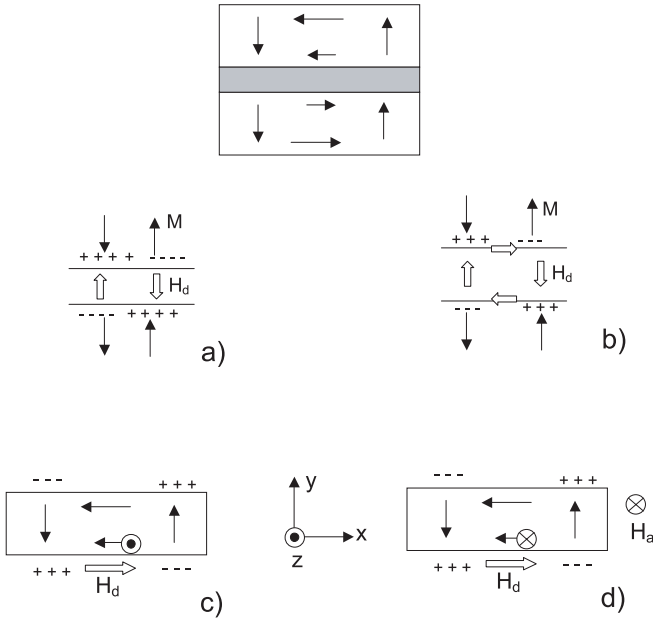

Fig. 14. Schematic representation of the demagnetizing field H_d near the non-magnetic spacer a) for a thin one and b) a larger one. c) details of the magnetization in the top magnetic-layer of the stack in the remanent state with rough indications of the demagnetizing field, d) same as c) when reversing the applied field, now along $-OZ$.

Due to the dipolar coupling effect, even in the absence of any interlayer exchange coupling, the bilayer can support a stripe pattern as long as the spacer is not too thick. Compared to a continuous film, this domain structure is characterized by a much smaller average longitudinal magnetization component resulting from the absence of a vortex core as well as a larger period of the pattern.

In the peculiar case of a very thin spacer, the magnetization in the remanent state is mainly transverse. Therefore no hysteresis is expected for such magnetic stack. Topological analysis has been done to support this important result. However, such characteristic behaviour disappears with thicker spacer mainly due to the presence of demagnetizing energy barrier occurring during magnetization reversal.

References

1. S. Hamada, N. Hosoito, T. Ono, T. Shinjo, J. Magn. Magn. Mater. **198-199**, 496 (1999).
2. K. Kano, K. Kagawa, A. Suzuki, A. Okabe, K. Hayashi, K. Aso, Appl. Phys. Lett. **63**, 2839 (1993).
3. W.F. Egelhoff, Jr., P.J. Chen, C.J. Powell, M.D. Stiles, R.D. McMichael, C.-L. Lin, J.M. Sivertsen, J.H. Judy, K. Takano, A.E. Berkowitz, T.C. Anthony, J.A. Brug, J. Appl. Phys. **79**, 5277 (1996).
4. H. Niedoba, B. Mirecki, M. Jackson, S. Jordan, S. Thompson, J.S.S. Whiting, P. Djémia, F. Ganot, P. Moch, T.P. Hase, I. Pape, B.K. Tanner, Phys. Stat. Sol. (a) **158**, 259 (1996).
5. M. Labrune, J. Miltat, J. Magn. Magn. Mater. **151**, 231 (1995).
6. M. Labrune, J. Miltat, J. Appl. Phys. **75**, 2156 (1994).
7. M. Labrune, H. Niedoba (unpublished).
8. P. Trouilloud, J. Miltat, J. Magn. Magn. Mater. **66**, 199 (1987).
9. M. Hehn, Ph.D. Thesis, University of Strasbourg (1997).
10. R. Ploessel, J.N. Chapman, M.R. Scheinfein, J.L. Blue, M. Mansuripur, H. Hoffmann, J. Appl. Phys. **74**, 7431 (1993).
11. A. Hubert, R. Schäfer, *Magnetic domains* (Springer, Berlin, 1998), p. 301.
12. E. Feldkeller, Z. Angew. Phys. **19**, 530 (1965).
13. M. Labrune, L. Belliard, Phys. Stat. Sol. (a) **174**, 483 (1999).
14. M. Labrune, A. Thiaville, Eur. Phys. J. B **23**, 17 (2001).
15. M.W. Muller, Phys. Rev. **122**, 1485 (1961).
16. A.P. Malozemoff, J.C. Slonczewski, in *Magnetic Domain Walls in Bubble Materials* (Academic, New York, 1979).